Gold nanostructures: engineering their plasmonic properties for biomedical applications

Min Hu,[ae] Jingyi Chen,[a] Zhi-Yuan Li,[b] Leslie Au,[a] Gregory V. Hartland,[c] Xingde Li,[d] Manuel Marquez[e] and Younan Xia*[a]

Received 6th July 2006
First published as an Advance Article on the web 6th September 2006
DOI: 10.1039/b517615h

The surface plasmon resonance peaks of gold nanostructures can be tuned from the visible to the near infrared region by controlling the shape and structure (solid *vs.* hollow). In this *tutorial review* we highlight this concept by comparing four typical examples: nanospheres, nanorods, nanoshells, and nanocages. A combination of this optical tunability with the inertness of gold makes gold nanostructures well suited for various biomedical applications.

Introduction

Gold nanostructures have been a subject of intensive research for their fascinating surface plasmon resonance (SPR) properties. What is SPR?[1] It is an optical phenomenon arising from the interaction between an electromagnetic wave and the conduction electrons in a metal. Under the irradiation of light, the conduction electrons in a gold nanostructure are driven by the electric field to collectively oscillate at a resonant frequency relative to the lattice of positive ions. At this resonant frequency, the incident light is absorbed by the nanostructure. Some of these photons will be released with the same frequency in all directions and this process is known as scattering. At the same time, some of these photons will be converted into phonons or vibrations of the lattice and this process is referred to as absorption. In general, the SPR peak of a gold nanostructure should include both scattering and absorption components. The cross-sections of these two components can be substantially different depending on the size and shape of the nanostructure. For gold nanospheres about 50 nm in diameter, the SPR peak is positioned at 520 nm, and this peak is responsible for the ruby red colour displayed by conventional gold colloids.[2] Michael Faraday was the first person to observe this spectacular phenomenon. In 1857, he prepared the first stable suspension of gold colloids by reducing gold chloride with phosphorus in water.[3] Some of his original samples are still preserved and on display at the Faraday Museum in London.

The SPR spectra of gold nanostructures can be calculated by solving Maxwell's equations. For spherical particles, this was accomplished in 1908 by Gustav Mie, a German physicist.[4] In 1912, Richard Gans modified the Mie theory to include spheroids.[5] Later, the capability of this theory was further extended to cover a number of other simple systems.[6] These days, one can still use the formulas derived by Mie to conveniently compute the SPR spectra (including both scattering and absorption) of a spherical particle in any size. However, since exact solutions to Maxwell's equations are known only for spheres, concentric spherical shells, spheroids, and infinite cylinders, an approximation is required to solve the equations for other geometries. The approximation of

[a]*Department of Chemistry, University of Washington, Seattle, WA 98195-1700, USA. E-mail: xia@chem.washington.edu*
[b]*Institute of Physics, Chinese Academy of Sciences, Beijing 100080, P. R. China*
[c]*Department of Chemistry and Biochemistry, University of Notre Dame, Notre Dame, IN 46556-5670, USA*
[d]*Department of Bioengineering, University of Washington, Seattle, WA 98195, USA*
[e]*INEST Group, Research Center, Philip Morris Inc., Richmond, VA 23234, USA*

Min Hu

Min Hu received his BS in Material Science and Engineering from the University of Science and Technology of China (USTC) in 2000. He received his PhD in physical chemistry from the University of Notre Dame (with Professor Gregory V. Hartland) in 2005. He is currently a Philip Morris USA INEST postdoctoral fellow with Marquez and Xia.

Jingyi Chen

Jingyi Chen received her BS degree in 1997 from the Sun Yat-Sen University in China and her MA degree (with Professor Kimberly A. Bagley) in 2002 from the Department of Chemistry, SUNY College at Buffalo. She is currently a PhD candidate in chemistry with Xia.

choice is based upon discrete dipole approximation (DDA). In principle, this numerical approach can be easily applied to gold nanostructures of any arbitrary shape.[7]

The SPR properties of gold nanostructures have found use in a rich variety of applications. Gold nanospheres, for example, have been used to make colourful glasses for over one thousand years. This is probably the first practical application of nanomaterials in history, although clearly the people who made the glasses had no idea about the mechanism of colouration. Another astonishing example comes from the Lycurgus cup (Roman 400 A.D.) which reflects green light and transmits ruby red light. This is again built upon the unique scattering and absorption properties of gold nanospheres embedded in the glass. In addition to these ancient demonstrations, gold colloids have also found extensive use in contemporary techniques such as colorimetric sensing[8] and surface-enhanced Raman scattering (SERS).[9] This tutorial review mainly focuses on the biomedical applications derived from the scattering and/or absorption power of gold nanostructures. A common feature of these applications is the use of near infrared light (800 nm to 1200 nm) to achieve deep penetration into soft tissues.[10] We begin with gold nanospheres to introduce the Mie theory, and then use nanorods, nanoshells, and nanocages as three typical examples to illustrate how their plasmonic peaks can be shifted from the visible to the near infrared region by engineering their shapes and structures (*i.e.*, solid *vs.* hollow). At the end, we highlight two innovative applications enabled by these novel gold nanostructures: optical contrast enhancement and photothermal treatment.

Gold nanospheres

Nanoparticles prepared in a solution phase tend to have a spherical shape because this shape has the smallest surface area relative to objects of other shapes (when the volume is fixed). It is worth noting that most of the gold nanospheres reported in literature are not in a truly spherical shape. They are multiply twinned particles with a more or less rounded profile and with facets on the surface. In a sense, these particles should be correctly called quasi-spheres. One of the most popular protocols for preparing gold nanospheres is based on the

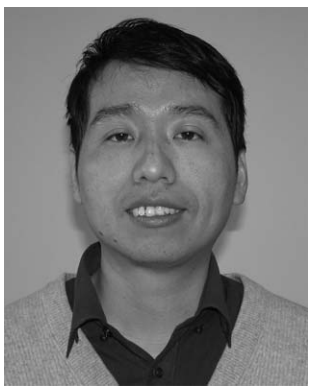

Zhi-Yuan Li

Professor Zhi-Yuan Li received his BS in optoelectronics from the University of Science and Technology of China (USTC) in 1994 and then worked as a graduate student on photonic crystals and near-field optics at the Institute of Physics, Chinese Academy of Sciences. After obtaining his PhD degree in 1999, he worked as a postdoctoral fellow at the Hong Kong University of Science and Technology, the University of Washington, and the Ames National Laboratory. He is currently a professor in the Institute of Physics at the Chinese Academy of Sciences in Beijing.

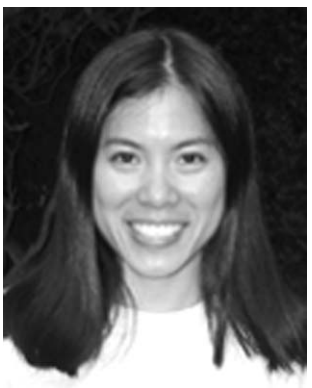

Leslie Au

Leslie Au attended the University of Washington and graduated in 2005 with a double BS degree in chemistry and biology. She is currently a PhD candidate in chemistry with Xia.

Gregory V. Hartland

Professor Gregory V. Hartland received his BSc in 1985 from the University of Melbourne, Australia. He obtained his PhD in physical chemistry from the University of California at Los Angeles (with Professor Peter Felker) in 1991. He then worked as a postdoctoral fellow at the University of Pennsylvania (1991–94) with Professor Hai-Lung Dai. He joined the faculty at the University of Notre Dame in 1994. He was promoted to Associate Professor in 2000 and Professor in 2004. He is currently a member of the Advisory Boards for the Journal of Physical Chemistry and Physical Chemistry Chemical Physics.

Xingde Li

Professor Xingde Li received his BS degree in physics from the University of Science and Technology of China (USTC) in 1990. He received his PhD degree in physics from the University of Pennsylvania (with Professor Arjun G. Yodh) in 1998. He then worked as a postdoctoral fellow at MIT (with Professor James G. Fujimoto). He started as an Assistant Professor of Bioengineering at the University of Washington in 2001.

reduction of $HAuCl_4$ by citrate in water, which was first described in 1951 by Turkevitch and is now commonly referred to as the "Turkevitch method".[11] In this method, citrate serves as both a reducing agent and an anionic stabilizer. It yields 15 nm nanospheres with a fairly narrow size distribution through the following reaction:

$$6AuCl_4^- + C_6H_8O_7 + 5H_2O \Rightarrow 6CO_2 + 24Cl^- + 6Au^0 + 18H^+ \quad \text{(i)}$$

The Turkevitch method has been modified by a number of groups to produce gold nanospheres with diameters ranging from 15 to 150 nm by either controlling the ratio of citrate to $HAuCl_4$[12] or employing a γ-radiation method.[13] Other reduction methods have also been developed to achieve a better control over the size and size uniformity, including the "Schmid method" published in 1981[14] and the "Brust–Schiffrin method" reported in 1994.[15] Seed-mediated growth is another technique frequently used for producing spherical nanoparticles of different sizes. Recently, Murphy and co-workers have demonstrated that the size of gold nanospheres could be tuned from 5 to 40 nm by controlling the ratio between the seed and the precursor.[16] Gold nanorods can also be conveniently generated by employing the seed-mediated growth method (vide infra). Because of space limit, readers who are interested in the synthesis of gold nanospheres can further refer to a recent review by Daniel and Astruc.[17]

The ruby red colour displayed by suspension of gold spherical nanoparticles can be quantitatively explained by considering the scattering of an electromagnetic wave from the nanoparticles. The light scattering theory falls into two categories.[18] The first one was developed by Lord Rayleigh, which is only applicable to small, spherical particles made of a dielectric (non-absorbing) material. The second one was derived by Gustav Mie, which represents a generic solution to scattering and it can be applied to spherical particles of any size and composed of an absorbing or non-absorbing material. Thus, Mie theory is most useful in describing the optical properties of metallic spherical particles. Mie theory is the exact solution to Maxwell's electromagnetic field equations for a plane wave interacting with a homogenous sphere of radius R with the same dielectric constant as bulk metal. The extinction cross-section (C_{ext}) of the spheres can be obtained as a series of multipole oscillations if the boundary conditions are specified. The extinction efficiency factor Q_{ext} is defined as the ratio of the extinction cross-section to the physical cross-sectional area (πR^2), and it is a sum of both scattering and absorption. In a more specific case, when the diameter of the spherical particle is much smaller than the wavelength of the radiation ($2R \ll \lambda$) and only dipole oscillation contributes to the extinction cross-section, the electrodynamic calculation can be simplified by ignoring high order terms. This gives the most popular form of Mie theory for spherical particles:[1]

$$C_{ext} = \frac{24\pi^2 R^3 \varepsilon_m^{3/2}}{\lambda} \frac{\varepsilon_2}{(\varepsilon_1 + 2\varepsilon_m)^2 + \varepsilon_2^2} \quad (1)$$

In this equation, ε_m is the dielectric constant of the surrounding medium, $\varepsilon = \varepsilon_1 + i\varepsilon_2$ is the complex dielectric constant of the particle. From eqn (1), a resonance peak occurs whenever the condition of $\varepsilon_1 = -2\varepsilon_m$ is satisfied. This is the SPR peak which accounts for the brilliant colours of various metal nanoparticles.

Fig. 1 shows the extinction spectra calculated using Mie theory for gold nanospheres of different sizes. Their SPR peaks are located at *ca.* 520 nm. The peak slightly shifts to the red and becomes broader as the particle diameter increases to 100 nm. The broadening can be attributed to enhanced

Manuel Marquez

Dr Manuel Marquez received his BSc and MSc degrees in chemistry from Simon Bolivar University in Venezuela. He obtained his PhD in organic chemistry from Yale University in 1996 (with Professor Kenneth Wiberg). He was a CAPIT Postdoctoral Fellow with Professor Steve Suib at UConn. In late 1999 he accepted a position as director (and founder) of the NanoteK Consortium (sponsored by Kraft Foods R&D). In 2005 he moved to PMUSA where he currently is the Group Leader of the Interdisciplinary Network of Emerging Science and Technologies (INEST). He is an Adjunct Professor in the Harrington Department of Bioengineering at Arizona State University as well as in the Mechanical Engineering, VCU, Richmond, VA. He is also a Guest Scientist at the Center for Theoretical and Computational Nanosciences, NIST, and at the Nanotechnology Center, Los Alamos National Laboratory. His major areas of research include molecular engineering, nanotechnology, nanoscale properties and microfluidics.

Younan Xia

Professor Younan Xia received his BS in chemical physics from the University of Science and Technology of China (USTC) in 1987. He received his MS degree in inorganic chemistry from the University of Pennsylvania (with Professor Alan G. MacDiarmid) in 1993, and PhD degree in physical chemistry from Harvard University (with Professor George M. Whitesides) in 1996, after which he stayed at Harvard and worked as a postdoctoral fellow with Professors George M. Whitesides and Mara Prentiss. He started at the University of Washington as an Assistant Professor of Chemistry in 1997 and was promoted to Professor in 2004. His research interests include nanostructured materials, photonic crystals, colloidal chemistry, self-assembly, surface modification, electrospinning, microfabrication, magnetic nanoparticles, and novel devices for photonics, optoelectronics, and displays.

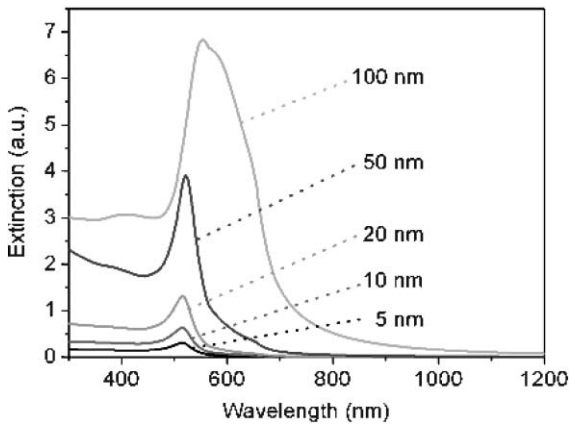

Fig. 1 Extinction spectra (Q_{ext}) calculated using Mie theory for gold nanospheres with diameters varying from 5 nm to 100 nm.

radiation damping for large particles. It is important to note that the position of SPR peak of gold nanospheres depends on the dielectric constant of environment, thus, different solvent or adsorption of a capping agent onto the nanospheres may result in slight variation for the SPR peak position. In addition, aggregation of gold nanospheres will lead to a pronounced colour transition from red to purple. This is due to plasmonic coupling between particles.[1] The colour changes are instrumental in fabricating colorimetric biosensors.[8]

Gold nanorods

Optical properties

The shape of a particle can drastically change the SPR properties. For nanorods, the boundary conditions in Mie theory have to be modified to describe their plasmonic properties. Unfortunately, it is not possible to obtain analytic expressions for particles with an arbitrary shape. In 1912, Gans modified Mie theory and predicted that for rod-shaped particles the SPR band would split into two modes due to different orientations of the rod with respect to the electric field of incident light.[5] According to Gans, the extinction cross-section can be expressed as:[5,19]

$$C_{ext} = \frac{2\pi V}{3\lambda}\varepsilon_m^{3/2}\sum_j \frac{\left(1/P_j^2\right)\varepsilon_2}{\left(\varepsilon_1 + \frac{1-P_j}{P_j}\varepsilon_m\right)^2 + \varepsilon_2^2} \quad (2)$$

where V is the volume of the rod, P_j ($j = A, B, C$; $A > B = C$, A = length, $B = C$ = width) are the depolarization factors for the elongated particles (nanorod), which are given by:

$$P_A = \frac{1-e^2}{e^2}\left[\frac{1}{2e}\ln\left(\frac{1+e}{1-e}\right) - 1\right] \quad (3a)$$

$$P_B = P_C = \frac{1-P_A}{2} \quad (3b)$$

where e is referred to as the rod ellipticity given by $e^2 = 1 - \xi^{-2}$, and ξ is the aspect-ratio (A.R.) of the nanorod ($\xi = A/B$). These equations can be used to calculate the extinction spectra of gold nanorods of any aspect-ratio, and the results were summarized by El-Sayed and co-workers.[19]

An alternative way to calculate the SPR spectra is based upon the DDA method. This numerical approach can, in principle, be applied to particles of any arbitrary shape.[7] In this calculation, the nanoparticle is treated as an array of N consecutive cells; each cell is approximated as a polarizable point dipole with a moment $\vec{\mathbf{P}}_i = \alpha_i \cdot \vec{\mathbf{E}}_{loc}(\vec{r}_i)$, where $\vec{\mathbf{E}}_{loc}$ is the local electromagnetic field of the ith point dipole at the position $\vec{r}_i$ and it has the contributions from the incident light field and all other dipoles in the particle. Once the position and polarizability of each individual cell have been specified, the absorption and scattering cross-sections of the particle can be determined. Fig. 2 shows a series of spectra calculated using the DDA method for gold nanorods with a fixed thickness of 20 nm but different aspect-ratios. The orientation of the nanorod must be specified in each calculation. In Fig. 2A, it is assumed the polarization of incident light is perpendicular to the axial direction of the nanorod, while in Fig. 2B it is parallel to that direction. These two separate bands are due to the electron oscillation across and along the long axis of the nanorod, respectively, and are therefore termed transverse and longitudinal modes accordingly. Note that the longitudinal plasmon band is continuously shifted from the visible to the near infrared region as the aspect-ratio of the nanorod increases. In contrast, the transverse resonance only shows a minor blue shift.

Synthesis of gold nanorods

A variety of methods have been demonstrated for preparing gold nanorods. For example, the template-directed method

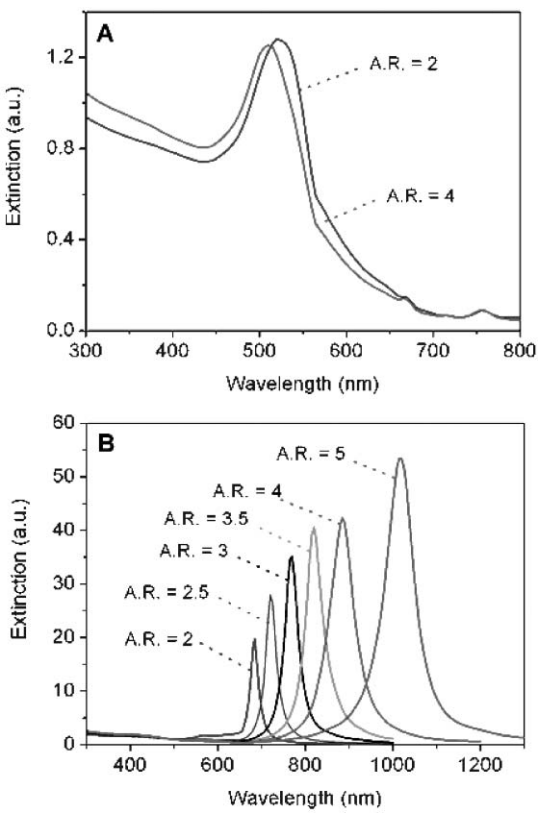

Fig. 2 Extinction spectra (Q_{ext}) calculated using the DDA method for gold nanorods of different aspect-ratios with a fixed width of 20 nm: (A) the transverse, and (B) longitudinal mode, respectively.

pioneered by Martin and others,[20] the electrochemical method introduced by Wang,[21] the seed-mediated growth method demonstrated by Murphy,[22] and the photochemical reduction method recently reported by Yang.[23] This review only covers the electrochemical and seed-mediated growth methods as these two methods have been commonly used.

Electrochemical method. This synthesis can be conducted in a simple, two-electrode cell, with a gold plate serving as the anode and a platinum plate as the cathode. Both metal electrodes are immersed in an electrolyte solution that contains a mixture of surfactants such as hexadecyltrimethylammonium bromide (C_{16}TAB) and tetradodecylammonium bromide (TC_{12}AB). The C_{16}TAB serves not only as a supporting electrolyte but also as a capping agent to prevent the nanoparticles from lateral growth while the TC_{12}AB acts as a rod-inducing agent. The electrolytic cell is then placed in an ultrasonic bath. A small amount of acetone and cyclohexane are added into the electrolytic solution before electrolysis. Acetone is used for weakening the micellar framework, and cyclohexane is necessary for facilitating the formation of elongated, rod-like C_{16}TAB micelles.[24] Electrolysis is carried out under a constant current mode for a typical period of 20 min. During the synthesis, the bulk gold metal is converted from the anode to gold complex ions $AuBr_4^-$, and these ions are driven by the current to the cathode. The reduction reaction takes place at the interfacial region between the cathode and the electrolytic solution. The gold complex ions may also combine with the cationic surfactants to facilitate the formation of rod-like gold nanoparticles.

To better control the aspect-ratio of the gold nanorods, an additional silver plate is added to the electrolytic solution. The $AuBr_4^-$ produced from the anode oxidizes the silver metal to ions (in the form of AgBr), and it is found that the concentration of silver ions and their release rate can affect the length of the nanorods. However, the detailed mechanism is still not very clear. Yang and co-workers proposed a mechanism to account for the role of the silver ions in the synthesis of gold nanorods using a photochemical method.[23] Briefly, silver exists in either AgBr or neutral cluster forms because of the competition between the photoreduction and chemical reactions with $AuCl_4^-$. This redox dynamics modulates the nascent surface of gold nanocrystals that are produced by UV reduction, and subsequently the growth rate along a particular direction is enhanced. It is believed by these authors that this mechanism is also shared by the electrochemical method when a silver electrode is involved.[23]

Seed-mediated growth method. A number of groups reported the use of seeds to facilitate the formation of monodispersed gold nanorods. Different reducing regents can be employed, such as hydroxylamine, sodium citrate, and ascorbic acid. A systematic study has recently been reported by Murphy and co-workers.[25] In a typical process, a solution of 3.5 nm gold seed particles is first prepared by reducing $HAuCl_4$ with sodium borohydride ($NaBH_4$) in the presence of citrate, which serves only as the capping agent since it cannot reduce gold salt at room temperature. A growth solution containing $HAuCl_4$ and C_{16}TAB is mixed with freshly prepared ascorbic acid solution (a mild reductant) and then added to a seed solution to generate gold nanorods. Although gold nanospheres are also formed in this synthesis, they can be readily removed (together with the excess surfactants) *via* centrifugation. Most recently, Mulvaney and co-workers investigated the factors affecting the formation of gold nanorods and modified the solution-phase synthesis to adjust the length of the rods from 25–170 nm.[26] Fig. 3 shows a typical TEM image of the gold nanorods as well as UV–Vis extinction spectra of such nanorods with different aspect-ratios from the Mulvaney group.[27] Note that the optical features of these experimentally synthesized nanorods are consistent with the spectra calculated using the DDA method.

The mechanism for the formation of rod-like nanoparticles in an aqueous surfactant medium has been investigated by several groups.[28,29] It was proposed that the trimethylammonium head group of C_{16}TAB can selectively bind to specific crystallographic facets of the seeds and/or rods, while the tails of C_{16}TAB can form a bilayer structure with each other through van der Waals interactions. These bilayers play an important role in promoting the formation of nanorods.[28] Experimental studies found that surfactants with longer chain lengths led to longer rods with higher yields as compared to shorter ones. Due to the limit of space, readers are encouraged to learn more current research into gold nanorods in a recent review.[30]

Gold nanoshells

Based on calculation, Neeves and Birnboim proposed in 1989 that a composite spherical particle consisting of a metallic shell and a dielectric core could give rise to SPR modes with their wavelengths tunable over a broad range of the electromagnetic spectrum.[31] Halas and co-workers were the first to produce gold nanoshells with SPR peaks in the near-infrared region by coating silica beads with gold shells of variable thickness.[32] They further demonstrated that the SPR peaks of gold nanoshells could be conveniently tuned by controlling the

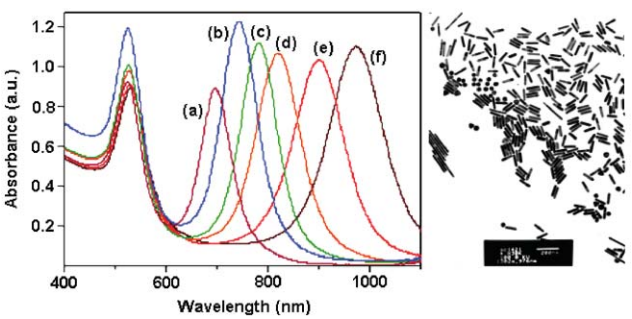

Fig. 3 UV–visible absorption spectra of Au nanorods with different aspect-ratios synthesized *via* citrate-capped seeds. The longitudinal peak shifts to the near-IR region as the amount of Au seeds decreases. The average lengths (L) and widths (w) for the different spectra are as follows: (a) $L = 46 \pm 6$ nm, $w = 20.7 \pm 2.3$ nm; (b) $L = 61 \pm 5$ nm, $w = 21.5 \pm 1.9$ nm; (c) $L = 73 \pm 4$ nm, $w = 22.1 \pm 1.5$ nm; (d) $L = 75 \pm 6$ nm, $w = 22.4 \pm 1.7$ nm; (e) $L = 89 \pm 7$ nm, $w = 22.2 \pm 2.0$ nm; (f) $L = 108 \pm 7$ nm, $w = 22.8 \pm 1.6$ nm. The right panel shows a representative TEM image of the sample corresponding to spectrum-f.

ratio of shell thickness to particle diameter.[33] Fig. 4 shows the SPR spectra of gold nanoshells calculated using the DDA method. In calculation, the diameter of the silica core was fixed at 60 nm and the shell thickness (t) was changed from 2 nm to 15 nm. Different from gold nanorods, the plasmonic properties of gold nanoshells are extremely sensitive to small variation in dimension (*i.e.*, shell thickness). For example, the SPR peak shifted from 870 nm to 1000 nm when the thickness of the shell was merely decreased by 1 nm, *i.e.*, from 3 nm to 2 nm. As expected, the dependence of the position of SPR peak on the shell thickness becomes much weaker when the shells become thicker.

Gold nanoshells are usually prepared by directly depositing gold onto silica colloidal spheres.[33,34] In a typical process, uniform silica spheres were first synthesized using the Stöber method, and their surfaces were then modified with a monolayer of amino-terminated silane such as 3-aminopropyltriethoxysilane. When a suspension of gold colloids with 1–2 nm in size was added, the particles were readily attached to the amine groups. Finally, more gold was deposited on the surface *via* chemical reduction to cover the silica core. Although this method has been actively explored as a generic route to dielectric/metallic core-shell particles, it is nontrivial to control the coverage, thickness, and smoothness of the metallic shells. Part of the reason can be attributed to the fact that most metals cannot wet the surface of an oxide material. In addition, metals such as gold and silver can easily grow into large particles once they have been nucleated. As a result, the metallic shells prepared using this method are usually characterized by big grain sizes and thus rough surfaces. In some cases, partially covered nanoshells (also known as nanocups) were obtained as the products.[35]

Gold nanocages

Gold nanocages represent a novel class of nanostructures that were recently developed by the Xia group.[36–40] Their SPR peaks can be tuned to the near infrared region by controlling the thickness and porosity of the walls. They can also be used as carriers of drugs and thus may have potential applications in drug delivery and/or controlled drug release. Furthermore, the hollow interiors can host small objects such as magnetic nanoparticles to construct multifunctional hybrid nanostructures.

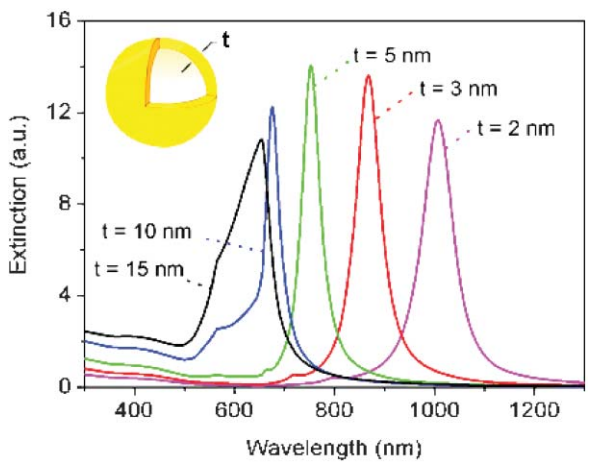

Fig. 4 The extinction spectra calculated for gold nanoshells supported on silica cores using DDA method. The diameter of the silica core is fixed at 60 nm while the shell thickness varies from 2 nm to 15 nm.

Tuning of the SPR peak

Although gold nanocages may have a complicated structure, they can be conveniently synthesized by templating against silver nanocubes through the well-known galvanic replacement reaction in a solution. The silver nanocubes are, in turn, synthesized using a polyol process,[41–45] in which a polyol (*e.g.*, ethylene glycol) serves as both solvent and reducing agent. In a typical synthesis, $AgNO_3$ is added to and reduced by ethylene glycol at an elevated temperature to generate silver nanocrystals (or seeds). More Ag atoms are then added to these seeds as $AgNO_3$ is continuously reduced. In the presence of poly(vinyl pyrrolidone) (PVP)—a polymer capable of selectively binding to the (100) surface—the addition of Ag atoms to the surface of the seeds can be directed to generate silver nanocrystals with well-defined and controllable shapes. In the synthesis of nanocubes, Ag atoms are preferentially added to the {111} facets of a single-crystal seed, leading to the formation of sharp corners. The silver nanocubes obtained are covered by PVP and can be separated from the reaction solution through centrifugation, and re-dispersed into water for subsequent applications. The seed crystallinity has a great impact on the yield of nanocubes.[42] Twinned seeds must be selectively removed *via* oxidative etching by combining oxygen from air and chloride. As a result, only single-crystal seeds are left in the system to grow into nanocubes of 30 to 200 nm in edge length, with size being mainly determined by reaction time. Fig. 5A shows TEM image of 30 nm silver nanocubes that were synthesized using the chloride-mediated polyol process. By optimizing experimental conditions, the dimensions of the silver nanocubes can also be reduced to the scale below 30 nm.

The driving force for the replacement reaction is due to the higher standard reduction potential of the $AuBr_4^-$/Au pair than the Ag^+/Ag pair. The chemical reaction involved in the galvanic replacement is the following:[37]

$$3Ag(s) + AuCl_4^-(aq) \Rightarrow Au(s) + 3Ag^+(aq) + 4Cl^-(aq) \quad (ii)$$

The mechanism of this replacement has been fully investigated. At the early stage, the silver nanocubes bounded by {100} facets reacted with the $HAuCl_4$ to form small holes on a specific face. As the replacement reaction continued, Au atoms resulting from the above reaction are epitaxially deposited on the surface of the silver nanocube to generate a thin shell. The Ag atoms can also diffuse into the gold shell, leading to the formation of a closed box made of Au–Ag alloy. Finally, the {111} facets at the corners of the nanoboxes were dealloyed and further etched when more $HAuCl_4$ solution was added. This eventually led to the formation of a hole at each corner of the nanobox. This porous structure can be clearly seen in the SEM and TEM images shown in Fig. 5B. The replacement reaction can be performed in a fashion similar to titration by adding a specific amount of the $HAuCl_4$

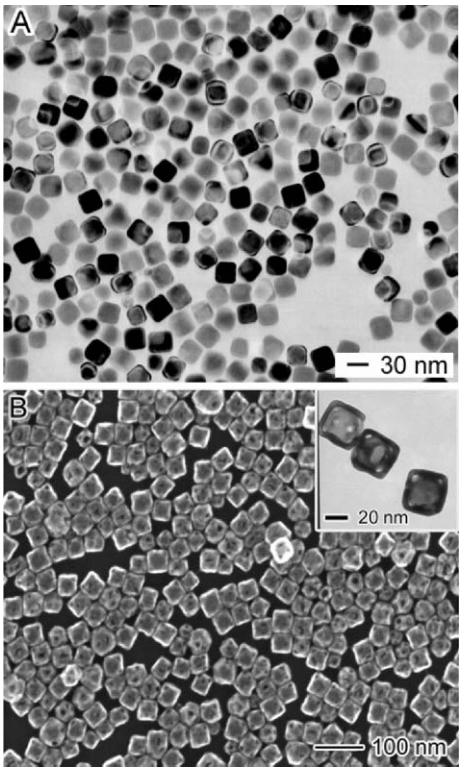

Fig. 5 (A) TEM image of the as-synthesized silver nanocubes with an edge length on the scale of 30 nm. (B) SEM image of gold nanocages (nanoboxes with truncated corners) prepared by refluxing an aqueous solution containing both silver nanocubes and $HAuCl_4$. The inset shows a TEM image of these hollow, porous nanostructures.

solution to the suspension of silver nanocubes. The size of the holes and the thickness of the walls can be easily adjusted by controlling the molar ratio of silver nanocubes to $HAuCl_4$. It is important to note that the galvanic replacement method can also be easily extended to templates in other shapes such as spheres and nanorods to produce a variety of functional nanostructures including single- or multiple-walled nanotubes.[37]

The SPR peaks of gold nanocages can be tuned by controlling the degree of galvanic replacement reaction to generate walls of different thicknesses and porosities. Fig. 6 shows aqueous solutions containing the gold nanocages, as well as their UV–Vis extinction spectra. The solutions were prepared by titrating 30 nm silver nanocubes with different volumes of 1 mM $HAuCl_4$ solution. It is clear that the positions of these SPR peaks could be continuously shifted from the visible (*ca.* 400 nm for silver nanocubes) to the near infrared region up to 1200 nm. Our DDA calculations indicate that the gold nanocages synthesized using the replacement reaction also have extremely large scattering and absorption cross-sections, implying their potential applications in biomedical imaging and photothermal therapy.[38–40]

Applications of gold nanostructures

The strong dependence of SPR peaks on local environment, as predicted by Mie theory and observed in many experiments, have made gold nanostructures attractive candidates for

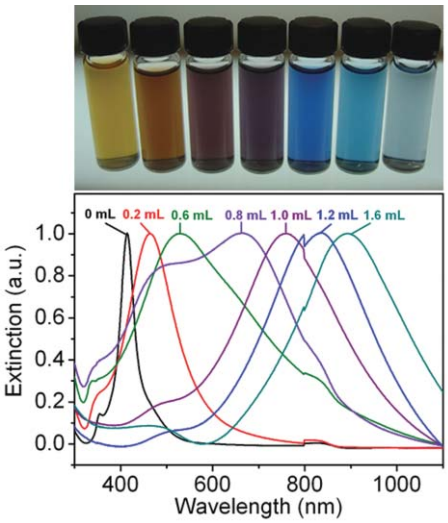

Fig. 6 Upper panel: vials containing gold nanocages (suspended in water) that were prepared by titrating silver nanocubes with different volumes of $HAuCl_4$ solution. Lower panel: extinction spectra recorded from aqueous suspensions of these gold nanocages, with the volume of $HAuCl_4$ solution labelled on each curve.

colorimetric sensors.[8,46] The great sensitivity of the SPR peaks also makes gold nanoparticles well-suited for bioassay applications.[47] The nanoparticle–protein conjugate structures include either direct binding of antigen or exposure of an antibody-derived surface to free antigen and then to a secondary antibody–Au–nanoparticle conjugate. This type of immunoassay has allowed the development of gold nanoparticle tags for antigen detection.[48] Analytes such as DNA, metal ions, and antibodies can all be detected by observing the visible colour changes due to metal nanoparticle aggregation. The detection mechanism is based on the change in optical properties due to plasmon–plasmon interaction between adjacent gold nanoparticles, which yields a colour change from characteristic ruby-red of gold colloid to a blue-purple color upon colloid aggregation. Because of the large scattering cross-sections of gold nanostructures, the Rayleigh resonance scattering can be detected using dark field microscopy. Van Duyne and co-workers recently demonstrated the use of gold nanoparticles as ''light scattering biochips'' for the selective detection of biomolecules.[49] Due to extremely large enhancement of the local electromagnetic field, the metal nanoparticles have been widely used as the substrates for surface-enhanced Raman scattering (SERS). This enhancement arises from two major mechanisms. The first one has a chemical origin, which is due to the formation of a charge-transfer complex between the surface and the analyte molecule. The second one can be attributed to the enhancement in electromagnetic field as a result of strong surface plasmon resonance of metal nanoparticle. The second mechanism plays a crucial role in the amplification of both the incident laser field and the scattered Raman field through their interaction with particle surface. Readers interested in SERS are recommended to explore more details from many reviews and books available on this subject.[50] Furthermore, the high absorption cross-section of gold nanoparticles has also enabled them to assist drug

delivery. For example, Halas and co-workers have shown that gold nanoshells loaded in hydrogels absorbed the near-infrared light, and the heat generated from the absorption caused the hydrogels to collapse, thus producing a modulated release of a soluble drug trapped in the hydrogel matrix.[51] For all these applications, it is an advantage to operate in the near-infrared region, a transparent window for blood and other types of biological samples.

Contrast enhancement for optical imaging

Like gold nanorods and nanoshells, the optical properties of gold nanocages can be precisely tuned to the specific wavelength in the electromagnetic spectrum. Compared with the former two nanostructures, nanocages can have stronger absorption in the near infrared while maintaining their relative small dimensions (*e.g.*, 30 nm in edge length). This feature makes gold nanocages a class of ideal contrast enhancement agents for use with optical imaging modalities like optical coherence tomography (OCT).[38] OCT is a technique based on the Michelson interferometer, which measures the interference signal between light backscattered from the sample and a reference beam. It is receiving great attention for its ability to perform high-resolution, non-invasive optical biopsies of tissue microanatomy. In conventional OCT, the envelope of interference fringes as well as the peak intensity of the envelope is displayed for tomographic imaging. Spectroscopic optical coherence tomography (SOCT), a technique for revealing the wavelength-dependent backscattering at a given position, measures the interference fringes (rather than the envelope). Spatially resolved spectra can be obtained by short-time Fourier transform (STFT) of the interferogram.[39] For both OCT and SOCT, the image contrast is mainly governed by intrinsic optical absorption and scattering of biological tissues. As a result, it is hard to resolve the minor morphological changes involved in the early stage development of a disease.

To demonstrate the potential of gold nanocages as contrast enhancement agents, both OCT and SOCT were performed on phantom samples with and without gold nanocages. The size of the nanocages is 35 nm and their SPR peak was tuned to 700 nm, which is on the blue side of the OCT source spectrum. Each phantom is made of gelatine embedded with TiO_2 granules to mimic the background scattering of typical biological tissues. In addition, the phantom is partially doped with gold nanocages at nM concentration. The OCT and SOCT imaging are conducted using a 7-fs Ti:Sapphire laser with a spectrum range from 700 nm to around 900 nm and the central wavelength is at 825 nm. As the laser was scanned over the tissue phantom, the intensity of back-scattered light was measured as a function of depth. Because of the intense absorption of the gold nanocages, a strong modulation of the back-scattered spectrum can be observed on the blue side, *i.e.*, at shorter wavelengths. Fig. 7A shows that the blue side of the source spectrum is attenuated more than the red side, producing a red-shift of the spectral centroid. Fig. 7B shows SOCT image of the phantom, displaying the spatially resolved centroid wavelength, which is encoded by hue. A red shift of the centroid is evident on the right-hand portion of the SOCT image, where the phantom was doped with gold nanocages,

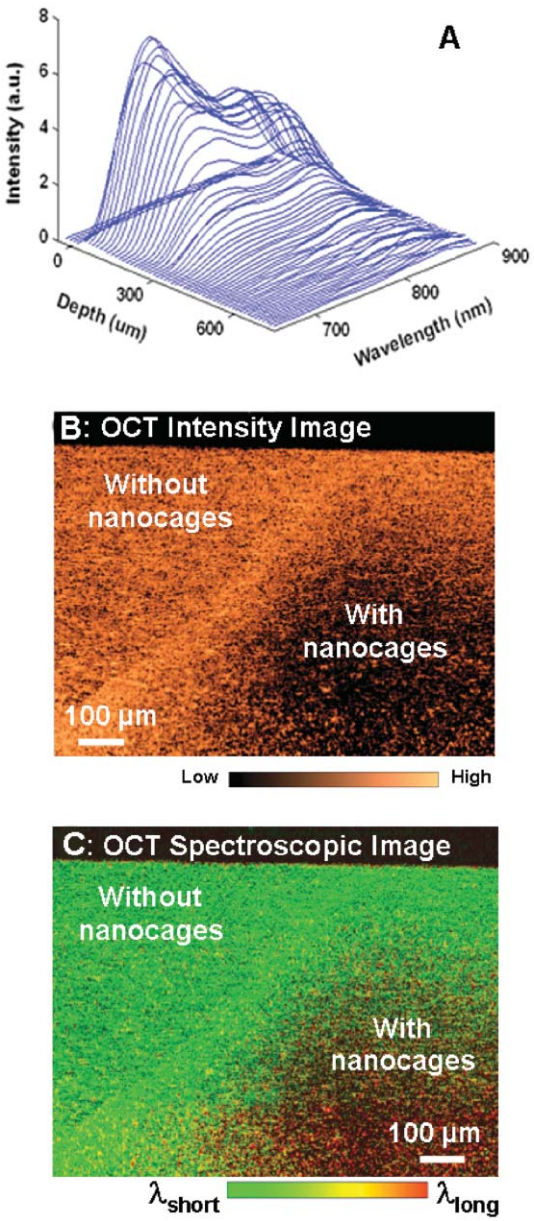

Fig. 7 (A) Spatially resolved spectra of the light backscattered from the phantom. Shorter wavelengths decay faster than longer ones, due to the stronger absorption of the nanocages at shorter wavelengths. (B) SOCT image of the phantom displaying the centroid of the spatially dependent backscattered spectra, which is mapped as hue. (C) HSV image that combines the intensity and spectroscopic content by encoding the OCT intensity as saturation and value and the centroid wavelength as hue.

demonstrating that the nanocages indeed enhanced the spectroscopic contrast. The contrast enhancement (*e.g.*, red-shift of the centroid) is stronger at greater depths owing to the increased absorption at shorter wavelengths by the nanocages.

In addition to the centroid SOCT image, the demodulated intensity (for OCT) and the spectroscopic centroid (for SOCT) can be combined into one image by using a hue-saturation-value (HSV) color map, with the centroid encoded into hue and the logarithm of the demodulated OCT intensity encoded into saturation and value. The HSV image is then converted to

a RGB (red-green-blue) image as shown in Fig. 7C, where a change in hue (*i.e.*, a red-shift) is accompanied by a decrease in image intensity in the right-hand portion of the image. On the other hand, the extinction cross-section of the gold nanocages can be quantified from the depth-dependent OCT intensity. To avoid contributions from multiple wavelengths to the extinction cross-section, only one wavelength at the resonance peak of the nanocages is presented. The depth-dependent OCT backscattered intensity at a single wavelength can be readily obtained from the spectroscopic OCT analysis. For the 35 nm gold nanocages, the absorption cross section determined from the experiments was 1.13×10^{-14} m^2, which is about 5 orders stronger than conventional dyes such as Indocyanine Green (ICG). This absorption cross section is of the same order of magnitude as gold nanoshells. However, the dimension of the nanocages is much smaller than the nanoshells. These results suggest that gold nanocages can serve as an excellent candidate of absorption contrast agents for OCT imaging. The extremely large absorption cross sections also indicate their use as an effective photothermal therapeutic agent.

Photothermal effect

Gold nanocages can be easily bioconjugated with antibodies for selective targeting of cancer cells. Exposure of the nanocages to light can convert the absorbed photons into phonons, leading to a temperature increase of the lattice. Heat dissipation from the hot particles may selectively cause damages to the targeted cancer cells.[40] This phenomenon is referred to as the photothermal effect of the metal nanoparticles and such an effect has been studied in an initial experiment by exposing gold nanocages supported on a copper grid to a camera flash. Each flash of light increased the temperature of the nanocages because they absorbed the incident photons. After exposure, the Au nanocages were transformed into solid spherical particles, indicating that the absorbed energies generated a lattice temperature beyond the melting point of the nanocages. This photothermally reshaping of the nanocages was attributed to the poor thermal conductivities of the surrounding materials (*e.g.*, air and thin carbon film on the TEM grid) which were in contact with the Au nanocages.

In biological system, the tissues and cells are essentially in a water environment, thus, the photothermal effect will be different. The photothermal properties of gold nanocages in an aqueous solution have been studied using ultrafast laser spectroscopy (or time-resolved spectroscopy).[52] In a typical experiment, a short pulse from a regeneratively amplified Ti:Sapphire laser was split into two components: pump and probe beams. The pump laser perturbs the absorption of the nanocages solution while the probe laser monitors the transient absorption induced by the former. The intense pump laser pulse excites the electrons and induces a hot electron distribution. Due to the small value for heat capacity of electrons, the temperature of the electron distribution can be very high. The electrons subsequently equilibrate with the lattice through an electron–phonon (e-ph) coupling process. This often occurs on a picosecond timescale, and has been extensively studied for spherical particles. Once the temperature of the electrons and lattice have equilibrated, the energy is transferred to the surroundings—which is water in the experiments—on a ten-to-hundred picoseconds timescale. On the other hand, the energy deposited by the laser pulses is channelled into the phonon mode. This increases the temperature of the lattice and causes the particle to expand. The time scale for heating is faster than the period of the phonon mode that correlates with the expansion coordinate, thus the vibrational mode can be coherently excited for nanocages.

By probing the vibrational period, one can get information of the lattice temperature created by laser excitation as well as the elastic constants of the materials. The latter is beyond the scope of this review and will not be addressed here. From the view point of physics, the softening of the vibrational period with increasing power is related to the temperature of the lattice, thus the temperature jump can be determined from the vibrational spectroscopy.[53] Fig. 8 shows transient absorption traces for the 68 nm gold nanocages under different excitation powers. The probe wavelength was 740 nm, which is near the SPR peak of the nanocages. The period increases approximately linearly with the pump laser intensity from 72 ps at low intensity to 77 ps at high intensity, as shown in the insert of Fig. 8. This experimental study shows that the nanocages maintain their structural integrity even at a laser intensity up to 17 μJ per pulse. The damage threshold of the nanocages was determined to be 20 μJ per pulse or above, *i.e.*, the nanocages were thermally reshaped at this power. Calibration experiments on Au nanospheres were performed to calculate the temperature jump in the nanocages. The results suggest that pump energy of 20 μJ per pulse creates a lattice temperature of 1200 ± 100 K in the nanocages, which is slightly below the melting point of the gold–silver alloy.

Heating with an ultrafast pulsed laser is much different from conventional thermal heating. Metal nanoparticles, like nanorods or nanocages, can be transformed into spherical

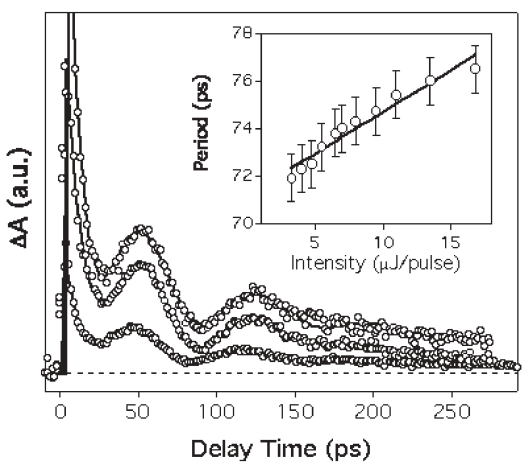

Fig. 8 Photothermal studies performed on the gold nanocages suspended in water solution. By probing the period changes in vibrational spectroscopy, the temperature jump in the nanocages after absorbing the pump laser energy can be determined to be around 1100 K with a laser power of 17 μJ per pulse.

particles upon thermal heating at a much lower temperature than their corresponding melting points, for example, the gold nanocages will become nanospheres at about 250 °C while they maintain their shapes under ultrafast laser pulse excitation with very high temperature jumps. The fact that the nanocages maintain their structure up to high lattice temperatures is good for photothermal therapy applications. The goal in photothermal therapy is to use near infrared light to image and kill cancer cells (for example) *via* selective heating. For this to work with metal nanoparticles, the particles must be stable under laser irradiation. The present work shows that for nanocages in solution, ultrafast laser excitation can create extremely high lattice temperatures without destroying the particles: The gold nanocages are still intact at 17 μJ per pulse, which corresponds to a lattice temperature around 1100 ± 100 K. This stability arises because of the rapid heat dissipation in solution. Note that thermally reshaping nanocages to spheres would greatly reduce their absorbance in the near infrared, and make them poor choices for photothermal therapy. In biomedical applications, the energy deposited by the laser will be directly transferred to the cell, creating a temperature jump far beyond where the cancer cell remains alive (*ca.* 330 K), eventually resulting in cell death. Thus, the combination of high repetition rate of near infrared, ultrafast laser sources with gold nanocages is very promising for photothermal therapy.

Concluding remarks

In the preceding sections, we have reviewed various approaches to engineering the plasmonic properties of gold nanostructures. Here we want to compare these different nanostructures in the context of biomedical applications where the exact magnitudes of both scattering and absorption are important. Fig. 9 compares the absorption, scattering, and extinction spectra calculated for gold nanorods, nanoshells, and nanocages using the DDA method. In these calculations, the dimensions of the structures were adjusted to tune their SPR peaks to 800 nm. This yields gold nanorods with an aspect-ratio of 3.3 and a fixed width (w) of 20 nm; gold nanoshells on silica cores with a core diameter (D_{core}) of 50 nm and shell thickness (t) of 3.2 nm; and gold nanocages with an inner edge length (D) of 50 nm and wall thickness (t) of 6 nm. The comparisons are based on the cross-sections because these parameters are directly related to the measured attenuation of light as the following:

$$M = \log_{10}(I_0/I_d) = kC_{ext}S/2.303 \quad (4)$$

where k is the number of particles per unit volume, I_0 and I_d are the intensities of incident light and transmitted light after passing through the sample, S is the optical path length of the sample cell. It is worth noting that the gold nanocages and nanorods have much larger absorption and scattering cross-sections than the gold nanoshells: *i.e.*, $C_{cage} \approx C_{rod} > C_{shell}$. Specifically, the extinction cross-sections of the nanocages or nanorods are more than 2 times stronger than that of nanoshells. Such high absorption cross-sections should make gold nanocages and nanorods better candidates than

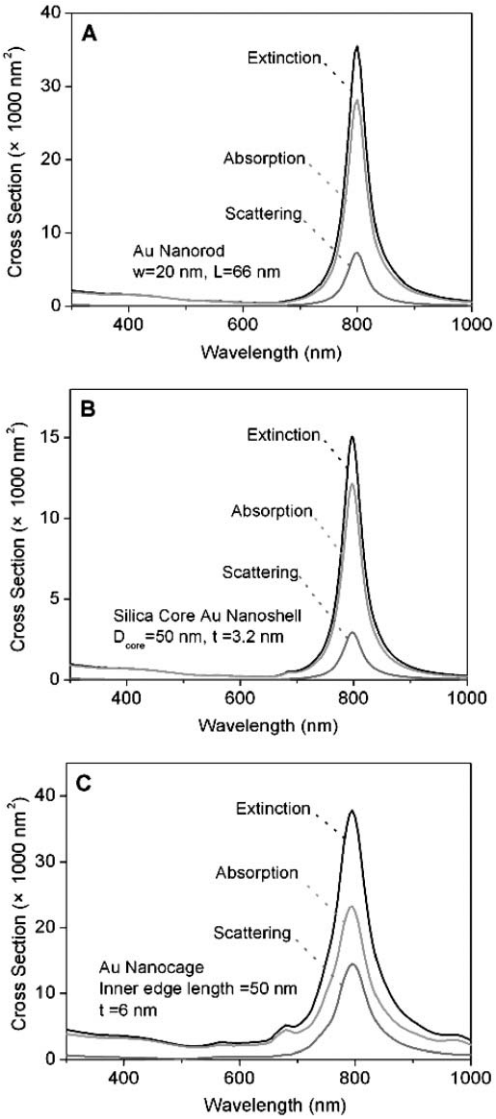

Fig. 9 Comparison of the optical spectra calculated using DDA for gold nanorods, nanoshells, and nanocages. For all the structures, the SPR peak was tuned to exactly 800 nm. (A) The gold nanorod has a width of w = 20 nm and length L = 66 nm. (B) The nanoshell has a silica core of 50 nm in diameter and shell thickness of 3.2 nm. (C) The nanocage has a water core with an inner edge length of 50 nm and wall thickness of 6 nm.

nanoshells for photothermal therapy as discussed in the previous section.

Gold nanostructures are of great interest for scientific research because of their attractive applications in photonics, electronics, optical sensing and imaging, and drug delivery. These interesting applications are built upon the fascinating SPR features of the nanostructures, a phenomenon that originates from the collective oscillation of conduction electrons relative to the lattice of gold ions. This optical property varies as a function of the size, shape, and hollowness/porosity of the nanostructures and can be readily calculated using Mie theory or DDA method. Parallel to the theoretical efforts, gold nanostructures with different shapes including nanospheres, nanorods, nanoshells, and nanocages

have been developed using various synthetic strategies. A combination of these efforts have recently established the agreement between the experimentally measured SPR spectra and those computed using the DDA method. The SPR peaks of these nanostructures can be tuned over a broad range from the visible to the near infrared. The remarkable SPR properties and biocompatibility of gold make them promising both as a contrast agent for *in vivo* optical imaging, and as a therapeutic agent for photothermal treatment of cancer.

Acknowledgements

This work has been supported in part by a DARPA-DURINT subcontract from Harvard University, a fellowship from the David and Lucile Packard Foundation, and the National Science Foundation. Y. X. is an Alfred P. Sloan Research Fellow (2000–2005) and a Camille Dreyfus Teacher Scholar (2002–2007). Z.-Y. L. was supported by the National Natural Science Foundation of China (No. 10525419). X. L. acknowledges the support from the NSF (Career Award). G. V. H. acknowledges the support of the Petroleum Research Fund administered by the American Chemical Society, and the NSF. We thank Prof. Paul Mulvaney and Jorge Pérez-Juste for allowing us to use Fig. 3 from their group.

References

1 U. Kreibig and M. Vollmer, *Optical Properties of Metal Clusters*, Springer, Berlin, 1995.
2 P. Mulvaney, *Langmuir*, 1996, **12**, 788.
3 M. Faraday, *Philos. Trans. R. Soc. London*, 1857, **147**, 145.
4 G. Mie, *Ann. Phys.*, 1908, **25**, 377.
5 R. Gans, *Ann. Phys.*, 1912, **37**, 881.
6 M. I. Mishchenko, W. J. Wiscombe, J. W. Hovenier and L. D. Travis, in: *Light Scattering by Nonspherical Particles: Theory, Measurements and Applications*, ed. M. I. Mishchenko, J. W. Hovenier and L. D. Travis, Academic Press, San Diego, 2000.
7 K. L. Kelly, E. Coronado, L. L. Zhao and G. C. Schatz, *J. Phys. Chem. B*, 2003, **107**, 668.
8 R. A. Reynolds, C. A. Mirkin and R. L. Letsinger, *J. Am. Chem. Soc.*, 2000, **122**, 3795.
9 P. M. Tessier, O. D. Velev, A. T. Kalambur, J. F. Rabolt, A. M. Lenhoff and E. W. Kaler, *J. Am. Chem. Soc.*, 2000, **122**, 9554.
10 J. L. West and N. J. Halas, *Annu. Rev. Biomed. Eng.*, 2003, **5**, 285.
11 J. Turkevitch, P. C. Stevenson and J. Hillier, *Discuss. Faraday Soc.*, 1951, **11**, 55.
12 M. A. Hayat, *Colloidal Gold: Principles, Methods and Applications*, Academic Press, San Diego, 1989.
13 A. Henglein and D. Meisel, *Langmuir*, 1998, **14**, 7392.
14 G. Schmid, R. Pfeil, R. Boese, F. Bandermann, S. Meyer, G. H. M. Calis and J. W. A. van der Velden, *Chem. Ber.*, 1981, **114**, 3634.
15 M. Brust, M. Walker, D. Bethell, D. J. Schiffrin and R. Whyman, *J. Chem. Soc., Chem. Commun.*, 1994, 801.
16 N. R. Jana, L. Gearheart and C. J. Murphy, *Chem. Mater.*, 2001, **13**, 2313.
17 M. C. Daniel and D. Astruc, *Chem. Rev.*, 2004, **104**, 293.
18 H. C. van de Hulst, *Light Scattering by Small Particles*, Dover Publications, New York, 1981.
19 S. Link and M. A. El-Sayed, *Int. Rev. Phys. Chem.*, 2000, **19**, 409 and references therein.
20 C. R. Martin, *Chem. Mater.*, 1996, **8**, 1739.
21 S. S. Chang, C. W. Shih, C. D. Chen, W. C. Lai and C. R. C. Wang, *Langmuir*, 1999, **15**, 701.
22 C. J. Murphy, T. K. Sau, A. M. Gole, C. J. Orendorff, J. X. Gao, L. F. Gou, S. E. Hunyadi and T. Li, *J. Phys. Chem. B*, 2005, **109**, 13857 and references therein.
23 F. Kim, J. H. Song and P. D. Yang, *J. Am. Chem. Soc.*, 2002, **124**, 14316.
24 M. Toernblom and U. Henriksson, *J. Phys. Chem. B*, 1997, **101**, 6028.
25 N. R. Jana, L. Gearheart and C. J. Murphy, *J. Phys. Chem. B*, 2001, **105**, 4065.
26 J. Pérez-Juste, L. M. Liz-Marzán, S. Carnie, D. Y. C. Chan and P. Mulvaney, *Adv. Funct. Mater.*, 2004, **14**, 571.
27 M. Hu, X. Wang, G. V. Hartland, P. Mulvaney, J. Pérez-Juste and J. E. Sader, *J. Am. Chem. Soc.*, 2003, **125**, 14925.
28 J. X. Gao, C. M. Bender and C. J. Murphy, *Langmuir*, 2003, **19**, 9065.
29 B. Nikoobakht and M. A. El-Sayed, *Langmuir*, 2001, **17**, 6368.
30 J. Pérez-Juste, I. Pastoriza-Santos, L. M. Liz-Marzán and P. Mulvaney, *Coord. Chem. Rev.*, 2005, **249**, 1870.
31 A. E. Neeves and M. H. Birnboim, *J. Opt. Soc. Am. B*, 1989, **6**, 787.
32 R. D. Averitt, D. Sarkar and N. J. Halas, *Phys. Rev. Lett.*, 1997, **78**, 4217.
33 S. J. Oldenburg, R. D. Averitt, S. L. Westcott and N. J. Halas, *Chem. Phys. Lett.*, 1998, **288**, 243.
34 R. D. Averitt, S. L. Westcott and N. J. Halas, *J. Opt. Soc. Am. B*, 1999, **16**, 1824.
35 C. Charnay, A. Lee, S. Q. Man, C. E. Moran, C. Radloff, R. K. Bradley and N. J. Halas, *J. Phys. Chem. B*, 2003, **107**, 7327.
36 Y. Sun and Y. Xia, *Science*, 2002, **298**, 2176.
37 Y. Sun and Y. Xia, *J. Am. Chem. Soc.*, 2004, **126**, 3892.
38 J. Chen, F. Saeki, B. J. Wiley, H. Cang, M. J. Cobb, Z. Y. Li, L. Au, H. Zhang, M. B. Kimmey, X. Li and Y. Xia, *Nano Lett.*, 2005, **5**, 473.
39 H. Cang, T. Sun, Z. Y. Li, J. Chen, B. J. Wiley, Y. Xia and X. Li, *Opt. Lett.*, 2005, **30**, 3048.
40 J. Chen, B. Wiley, Z. Y. Li, D. Campbell, F. Saeki, H. Cang, L. Au, J. Lee, X. Li and Y. Xia, *Adv. Mater.*, 2005, **17**, 2255.
41 F. Fievet, J. P. Lagier and M. Figlarz, *MRS Bull.*, 1989, **14**, 29.
42 B. Wiley, T. Herricks, Y. Sun and Y. Xia, *Nano Lett.*, 2004, **4**, 1733.
43 B. Wiley, Y. Sun, B. Mayers and Y. Xia, *Chem.-Eur. J.*, 2005, **11**, 454.
44 S. H. Im, Y. T. Lee, B. Wiley and Y. Xia, *Angew. Chem., Int. Ed.*, 2005, **44**, 2154.
45 B. Wiley, Y. Sun, J. Chen, H. Cang, Z.-Y. Li, X. Li and Y. Xia, *MRS Bull.*, 2005, **30**, 356.
46 J. W. Liu and Y. Lu, *J. Fluoresc.*, 2004, **14**, 343.
47 S. J. Oldenburg, C. C. Genick, K. A. Clark and D. A. Schultz, *Anal. Biochem.*, 2002, **309**, 109.
48 N. T. K. Thanh and Z. Rosenzweig, *Anal. Chem.*, 2002, **74**, 1624.
49 A. D. McFarland and R. P. Van Duyne, *Nano Lett.*, 2003, **3**, 1057.
50 Z. Q. Tian, B. Ren and D. Y. Wu, *J. Phys. Chem. B*, 2002, **106**, 9463 and references therein.
51 S. R. Sershen, S. L. Westcott, N. J. Halas and J. L. West, *J. Biomed. Mater. Res.*, 2000, **51**, 293.
52 M. Hu, H. Petrova, J. Chen, J. M. McLellan, A. R. Siekkinen, M. Marquez, X. Li, Y. Xia and G. V. Hartland, *J. Phys. Chem. B*, 2006, **110**, 1520.
53 G. V. Hartland, *Phys. Chem. Chem. Phys.*, 2004, **6**, 5263.

